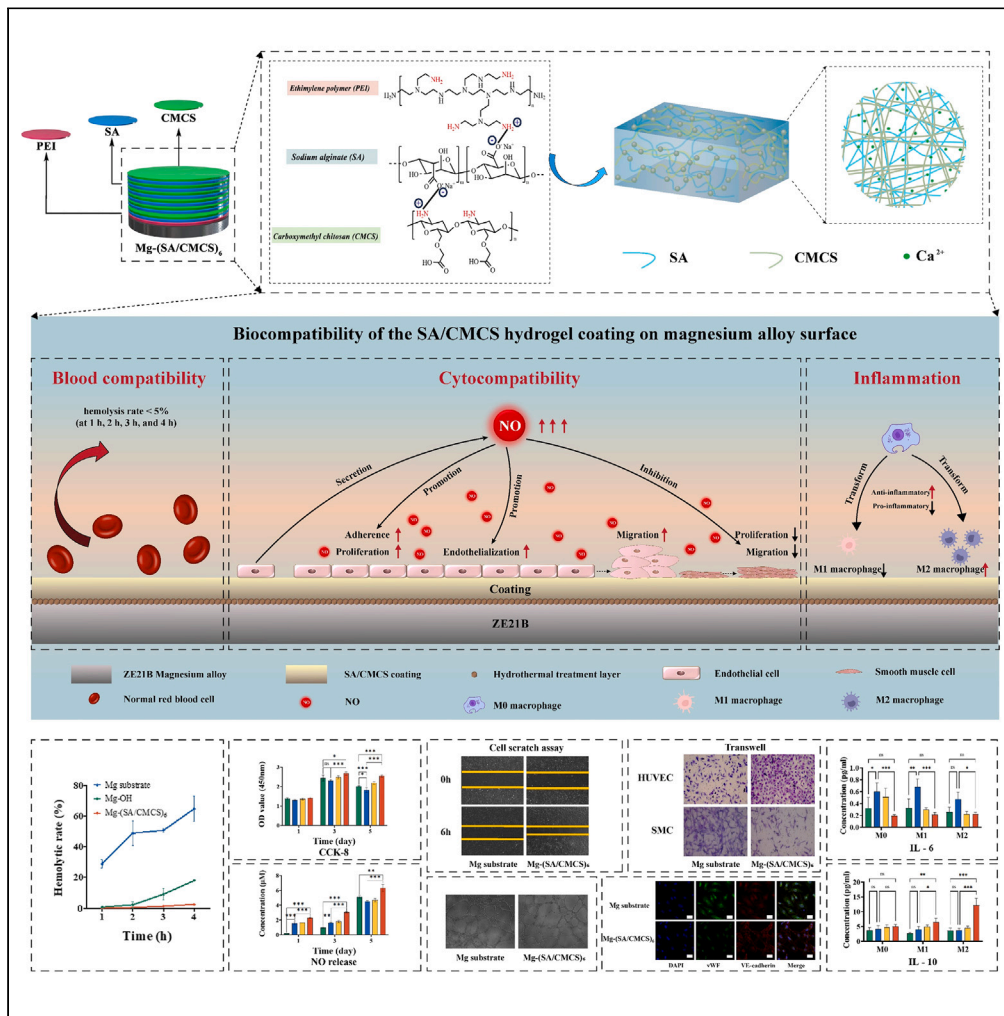**Article**

Preparation of biocompatibility coating on magnesium alloy surface by sodium alginate and carboxymethyl chitosan hydrogel

Rufeng Jia, Yanyan He, Jia Liang, ..., Huixia Cao, Tianxiao Li, Yingkun He

dr.litianxiao@zzu.edu.cn (T.L.)
heyingkun@zzu.edu.cn (Y.H.)

Highlights

Exhibit a lower hemolysis rate

Promote NO release from HUVECs more effectively

Facilitate the proliferation, migration and neovascularization of endothelial cells

Reduce M1 polarization and promote M2 polarization

Article

Preparation of biocompatibility coating on magnesium alloy surface by sodium alginate and carboxymethyl chitosan hydrogel

Rufeng Jia,[1,2,6] Yanyan He,[1,2,6] Jia Liang,[1,2,6] Lin Duan,[2,3] Chi Ma,[1,2] Taoyuan Lu,[1,2] Wenbo Liu,[1,2] Shikai Li,[2] Haigang Wu,[4] Huixia Cao,[5] Tianxiao Li,[1,2,3,*] and Yingkun He[1,2,7,*]

SUMMARY

Magnesium alloy is an excellent material for biodegradable cerebrovascular stents. However, the rapid degradation rate of magnesium alloy will make stent unstable. To improve the biocompatibility of magnesium alloy, in this study, biodegradable sodium alginate and carboxymethyl chitosan (SA/CMCS) was used to coat onto hydrothermally treated the surface of magnesium alloy by a dipping coating method. The results show that the SA/CMCS coating facilitates the growth, proliferation, and migration of endothelial cells and promotes neovascularization. Moreover, the SA/CMCS coating suppresses macrophage activation while promoting their transformation into M2 type macrophages. Overall, the SA/CMCS coating demonstrates positive effects on the safety and biocompatibility of magnesium alloy after implantation, and provide a promising therapy for the treatment of intracranial atherosclerotic stenosis in the future.

INTRODUCTION

Intracranial atherosclerotic stenosis (ICAS) is a significant contributor to the occurrence and recurrence of ischemic stroke worldwide.[1] The advent of intracranial endovascular stents has provided a therapeutic option for the interventional treatment of ICAS, gaining widespread use in clinical practice.[2,3] Magnesium alloy, characterized by its excellent mechanical properties and biocompatibility,[4–10] represents an ideal material for biodegradable stent.[11–13] However, there remain several challenges associated with the use of magnesium alloy as intracranial stent material. Rapid degradation of magnesium alloy often leads to excessive corrosion products, resulting in elevated levels of Mg^{2+} ions and localized alkalinization that can induce cell death. Additionally, inadequate surface endothelialization and severe inflammatory reactions further limit their clinical application.[14,15]

Surface modification techniques provide a promising solution for enhancing the biocompatibility of magnesium alloy intracranial stents by applying corrosion-resistant coatings, including metal oxide, metal hydroxide, inorganic non-metal, polymer, or organic coatings.[16–28] Among these techniques, polymers or organic coatings have gained significant prominence in the field of stent coating materials compared to inorganic coatings due to their inherent biodegradability, exceptional biocompatibility, and ability to modulate cellular responses (e.g., adhesion, proliferation, and differentiation). Currently, widely utilized biodegradable materials primarily encompass natural degradable polymers (such as collagen,[21,22] chitosan,[23,24] and sodium alginate[25,26]) or synthetic degradable polymers (such as polylactic acid (PLA), poly-L-lactic acid (PLLA), poly(lactic-co-glycolic acid) (PLGA), and polycaprolactone (PCL)).[27,28]

Carboxymethyl chitosan (CMCS) is a water-soluble derivative of chitosan (CHI) that possesses favorable physiological properties.[29–32] Its low cytotoxicity and hydrophilic surface promote cell adhesion and proliferation, making it an ideal biological coating material.[33,34] Bakhsheshi-Rad et al.[23] applied electrospun chitosan nanofibers to the surface of Mg-Zn-Ca alloy, thereby enhancing its biocompatibility and corrosion resistance of the alloy. Córdoba et al.[21,22] successfully developed a bilayer silane-titanium dioxide/chitosan coating on magnesium alloy, which facilitated cell proliferation. Cui et al.[24] achieved successful preparation of a chitosan/DNA self-assembly coating on the AZ31 alloy surface, demonstrating favorable cytocompatibility, antibacterial activity, and corrosion resistance.

[1]Department of Cerebrovascular Disease, Zhengzhou University People's Hospital, Henan Provincial People's Hospital, Zhengzhou, Henan 450003, China
[2]Henan Provincial NeuroInterventional Engineering Research Center, Henan International Joint Laboratory of Cerebrovascular Disease, and Henan Engineering Research Center of Cerebrovascular Intervention Innovation, Zhengzhou, Henan 450003, China
[3]Department of Neurosurgery, Zhengzhou University People's Hospital, Henan Provincial People's Hospital, Zhengzhou, Henan 450003, China
[4]School of Life Sciences, Henan University, Kaifeng, Henan 475004, China
[5]Department of Nephrology, Henan Provincial Key Laboratory of Kidney Disease and Immunology, Zhengzhou University People's Hospital, Henan Provincial People's Hospital, Zhengzhou, Henan 450003, China
[6]These authors contributed equally
[7]Lead contact
*Correspondence: dr.litianxiao@zzu.edu.cn (T.L.), heyingkun@zzu.edu.cn (Y.H.)
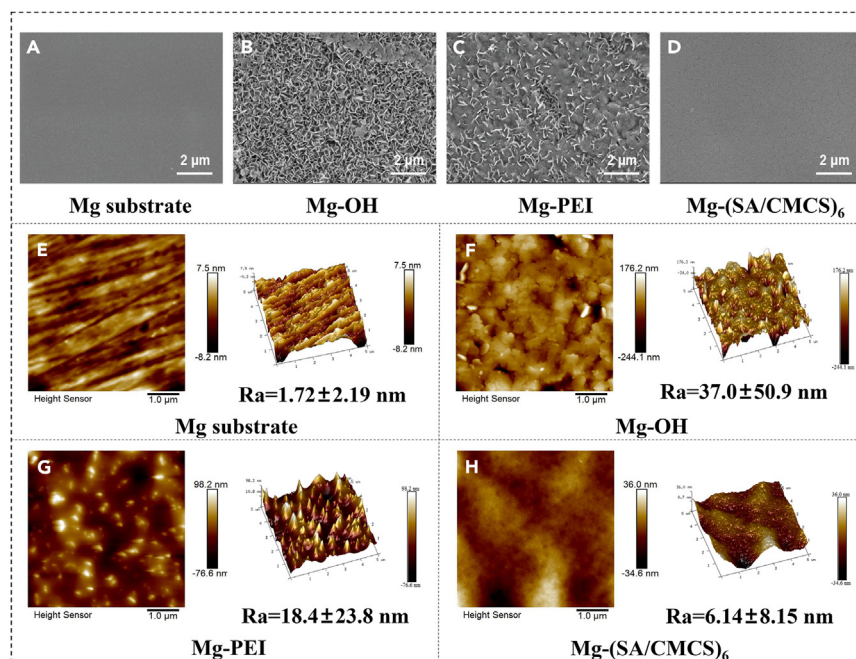https://doi.org/10.1016/j.isci.2024.109197

Figure 1. SEM, AFM plot of the sample

SEM image of (A) Mg substrate, (B) Mg-OH, (C) Mg-PEI, (D) Mg-(SA/CMCS)$_6$ coatings (scale bar = 2 μm); AFM image of (E) Mg substrate, (F) Mg-OH, (G) Mg-PEI, (H) Mg-(SA/CMCS)$_6$ coatings (scale bar = 1 μm).

Sodium alginate (SA), a naturally occurring polymer with excellent biocompatibility and biodegradability, is widely utilized in various applications.[30,35,36] An aqueous solution of SA forms a highly viscous liquid composed of molecules linked by β-D-mannuronic (M) and α-L-guluronic (G) bonds (1→4). In the presence of Ca^{2+} ions, the Na^+ ions on the G unit undergo ion exchange with divalent cations, resulting in the accumulation of the G unit and formation of a cross-linked network structure that leads to hydrogel formation.[37–41] Qiang Zou et al.[26] conducted a study involving the prevascularization of 3D printed vascular stent by premixing human umbilical vein endothelial cells (HUVECs) in a SA hydrogel and spraying them onto the stent. The results demonstrated cell proliferation within the stent while maintaining favorable biological characteristics. Once gelation occurs, SA firmly adheres to the surface of the magnesium substrate, preventing coating detachment. Furthermore, this gelation condition preserves activity levels for substances such as cells,[42] sensitive drugs,[43] proteins,[44] and enzymes,[45] thereby significantly enhancing coating biocompatibility.

The ZE21B (Mg-2.0Zn-0.5Y-0.5Nd) magnesium alloy was employed as the substrate material for design and fabricate an SA/CMCS coating, which could be applied to the biodegradable ZE21B magnesium alloy material.[4–10] Initially, a hydrothermal treatment was conducted to form a chemical conversion layer of Mg(OH)$_2$ on the surface of magnesium alloy. Subsequently, a dipping coating method was utilized to sequentially coat SA/CMCS onto the surface of the magnesium alloy. The morphology and structure of the coated surface were characterized using scanning electron microscopy (SEM), Atomic force microscopy (AFM), X-ray photoelectron spectroscopy (XPS), and X-ray diffractometer (XRD) analysis techniques. Electrochemical tests, Mg^{2+} detection, and pH measurement in solution were performed to investigate the corrosion resistance of the coated magnesium alloy. Furthermore, contact angle measurements and hemocompatibility tests were carried out to evaluate the hydrophobicity and hemocompatibility of the coating surface respectively. To verify its biocompatibility effects on vascular endothelium, smooth muscle cells (SMCs), and inflammation response under normal culture conditions as well as in presence of magnesium alloy extract, we compared proliferation, migration, and inflammatory responses of human umbilical vein endothelial cells (HUVECs), human coronary artery smooth muscle cells (HCASMCs) and macrophages.

RESULTS

Morphology and structure characterization of magnesium alloy surface coating

The surface morphology and roughness of the coatings were characterized by SEM and AFM, and the results are shown in Figure 1. After mechanical polishing, magnesium alloy exhibited a flat surface with a roughness of approximately 1.72 ± 2.19 nm (Figure 1E). The surface of magnesium alloy reacted with ultrapure water at high temperature and high pressure, forming a uniform lamellar crystalline structure, and the roughness increased to 37.0 ± 50.9 nm (Figure 1F). Then the samples were soaked in a 10 mg/mL PEI aqueous solution and dried, resulting in the formation of a PEI coating on the surface. SEM images revealed the presence of polymer on the sample surface, although it was not completely covered. AFM analysis showed a reduced surface roughness of 18.4 ± 23.8 nm (Figure 1G). After six cycles of dipping in an aqueous solution of SA and CMCS, the surface of sample was fully covered by the polymer (Figure 1D), resulting in a flat surface with a roughness of 6.14 ± 8.15 nm (Figure 1H).
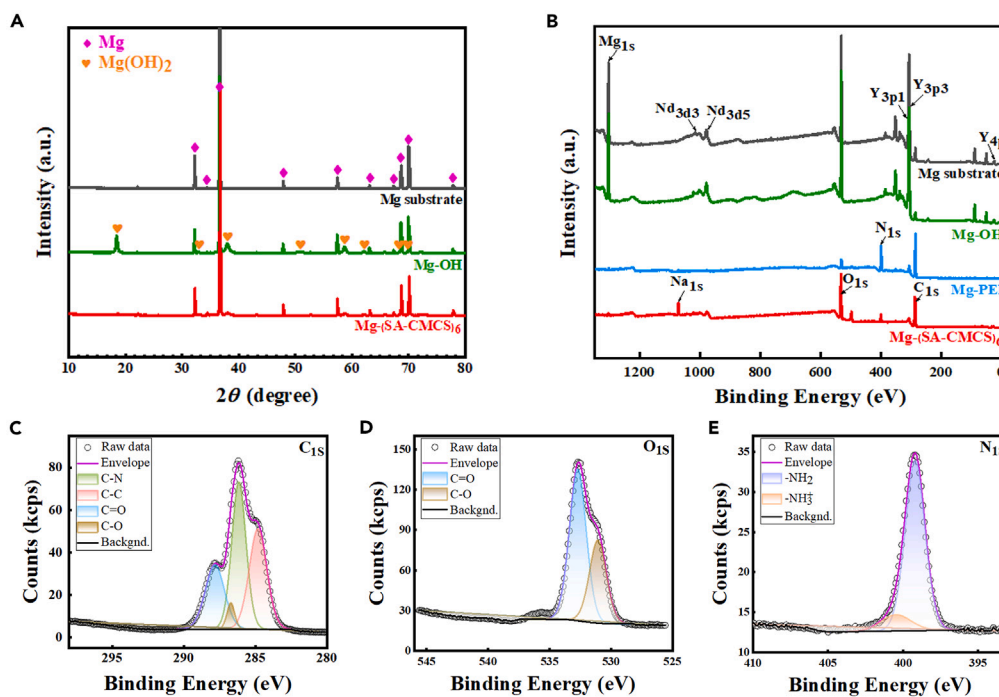
Figure 2. XRD, XPS plot of the sample

(A) XRD patterns of the Mg substrate, Mg-OH and Mg-(SA/CMCS)$_6$ coatings; (B) XPS spectra of Mg substrate, Mg-OH, Mg-PEI and Mg-(SA/CMCS)$_6$ coatings; The XPS spectra image of Mg after SA/CMCS coating: (C) C$_{1s}$, (D) O$_{1s}$, and (E) N$_{1s}$.

Figure 2 presents the XRD and XPS patterns of the Mg substrate, Mg-OH, Mg-PEI, and Mg-(SA/CMCS)$_6$ coated samples. XRD patterns illustrates the phase changes of the sample from the magnesium alloy to the hydrothermal treatment and subsequent coating (Figure 2A). The hydrothermal treatment led to the appearance of Mg(OH)$_2$. Figure 2B displays the XPS spectra for each layer during the coating preparation. The untreated magnesium alloy spectra exhibited characteristic peaks corresponding to the alloy elements of ZE21B magnesium alloy, such as Zn, Y, and Nd. After the hydrothermal treatment, an O$_{1s}$ characteristic peak appeared. Upon PEI dipping, the characteristic peak of the metal elements disappeared due to the formation of a polymer coating layer on the surface. Since PEI contains N elements, a significant increase in the N$_{1s}$ peak was observed. The Na$_{1s}$ peak started to appear after SA dipping, accompanied by changes in the N$_{1s}$ peak. The XPS peak-splitting analysis of the coated samples revealed four peaks in the C$_{1s}$ spectrum (Figure 2C): 284.8 eV (C-C/C-H), 286.1 eV (C-N), 286.7 eV (C-O), and 287.9 eV (C=O). The O$_{1s}$ spectrum (Figure 2D) showed two peaks: one (C-O) at 532.7 eV and the other (C=O) at 531.3 eV. The N$_{1s}$ spectrum exhibited two split peaks in the multilayer film (Figure 2E), with a peak of -NH$_2$ at 399.1 eV and a peak of -NH$_3^+$ at 400.4 eV. The adhesion test showed that the adhesion force of the coating increased after ethylene imine polymer treatment (Figure S1).

Coating properties

Electrochemical

Electrochemical test is a typical method to evaluate the metals' degradability. Polarization curve is a common tool to assess the instantaneous corrosion rate of metal and to evaluate the corrosion resistance of protective coatings on metal substrate. To investigate the protective efficacy of Mg-OH, and Mg-(SA/CMCS)$_6$ samples, these samples were immersed in SBF for 1 h, followed by electrochemical measurements. The Tafel curves of the Mg substrate, Mg-OH, and Mg-(SA/CMCS)$_6$ samples are presented in Figure 3, and the electrochemical parameters (mean ± SD) derived from the Tafel curves are displayed in Table 1. From Figure 3, it is evident that the corrosion performance of the magnesium alloy, after hydrothermal treatment and coating, differs among the metal samples. The bare magnesium alloy exhibits the smallest E$_{corr}$ (−1.736 V) and the largest i$_{corr}$ (1.451 × 10^{-4} A·cm^{-2}). In contrast, the Mg-(SA/CMCS)$_6$ sample, following surface modification with the coating, displays a larger E$_{corr}$ (−1.506 V) and a smaller i$_{corr}$ (2.488 × 10^{-7} A·cm^{-2}) compared to the bare magnesium alloy. After hydrothermal treatment, the i$_{corr}$ (1.228 × 10^{-5} A·cm^{-2}) of the Mg-OH sample falls between that of the bare magnesium alloy and the Mg-(SA/CMCS)$_6$ sample, and the E$_{corr}$ (−1.491 V) of the Mg-OH sample is equivalent to that of the Mg-(SA/CMCS)$_6$ sample.

Mg^{2+} concentration and pH value

By immersing different groups of samples directly in simulated body fluid (SBF) and measuring the changes in Mg^{2+} concentration and pH value of the soaking solution (Figure 4), it was observed that the bare magnesium alloy exhibited significant variations in Mg^{2+} concentration
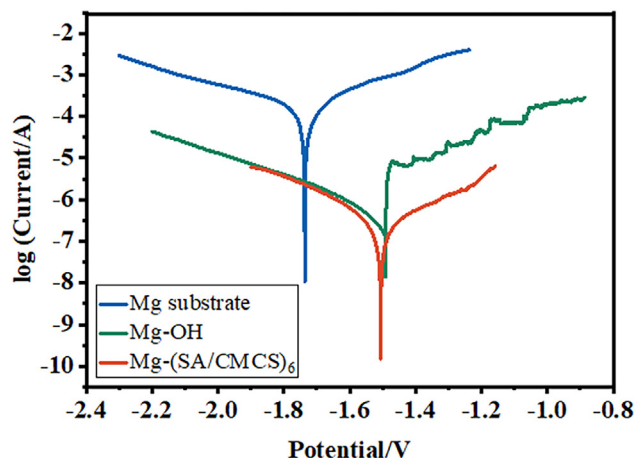
Figure 3. Tafel curves of Mg substrate, Mg-OH, and Mg-(SA/CMCS)$_6$ samples in SBF

and pH value from 0 h to 6 h after immersion in SBF. Conversely, the Mg^{2+} concentration and pH value of the Mg-OH group (treated with hydrothermal treatment) and the Mg-(SA/CMCS)$_6$ group (modified with the coating surface) showed minimal changes, with only a slight increase. After 8 h, the changes in Mg^{2+} concentration and pH value in the bare magnesium alloy group samples became smoother, while the Mg^{2+} concentration and pH value in the Mg-OH group samples exhibited significant fluctuations. Furthermore, the Mg^{2+} concentration and pH value in the Mg-(SA/CMCS)$_6$ group samples changed gradually following the surface modification, and they were significantly lower than those of the bare magnesium alloy and Mg-OH group samples.

Hydrophilicity and hemocompatibility

The water contact angle (Figure 5A) of the surface-polished magnesium alloy is 71.54 ± 0.80°. Upon hydrothermal treatment, a Mg(OH)$_2$ layer forms on the surface, leading to an increase in surface hydrophilicity to 19.78 ± 0.12°. Due to the hydrophilic properties of both SA and CMCS, the modified sample retains a highly hydrophilic surface, with a hydrophilic contact angle of approximately 36.13 ± 0.65°.

Subsequently, the Mg substrate, Mg-OH, and Mg-(SA/CMCS)$_6$ samples were incubated with a red blood cell suspension at 37°C for 1 h, 2 h, 3 h, and 4 h to assess red blood cell lysis upon contact with the samples, as shown in Figure 5B. Compared to the bare magnesium alloy, Mg-(SA/CMCS)$_6$ sample exhibit favorable anti-hemolytic properties. The hemolysis rate (mean ± SD) of Mg-(SA/CMCS)$_6$ at 1 h, 2 h, 3 h, and 4 h was 0.154 ± 0.117%, 0.557 ± 0.576%, 1.373 ± 0.559%, and 2.532 ± 0.333%, respectively. These values were lower than the International Organization for Standardization (ISO) standard for hemolytic properties of materials (5%) and met the requirements for clinical implantation.

Cytocompatibility
Effect of coating on endothelial cell proliferation and migration

The impact of coating on the growth, proliferation, and migration of vascular endothelial cells were investigated. The CCK-8 results (Figure 6A) demonstrated the proliferation of HUVECs cultured in extracts from bare magnesium alloy, hydrothermal treatment, and coating samples. After 1 day of culture, there was no significant difference in cell proliferation among the Control, Mg substrate, Mg-OH, and Mg-(SA/CMCS)$_6$ groups. However, after 3 and 5 days of culture, the SA/CMCS coating group exhibited enhanced cell proliferation compared to the Control, Mg substrate, and Mg-OH groups. Figure 6B presents the release of nitric oxide (NO) from HUVECs cultured for 1 day, 3 days, and 5 days in the culture medium and extracts of Mg substrate, Mg-OH, and Mg-(SA/CMCS)$_6$. The results revealed that the mean NO release in the Mg-(SA/CMCS)$_6$ group was 1.5 times higher than that in the Mg substrate group after 1 day of culture, 1.9 times higher after 3 days, and 1.4 times higher after 5 days. Furthermore, NO release gradually increased with the extension of culture time, with the Mg-(SA/CMCS)$_6$ group demonstrating higher NO release, indicating its superior promotion of NO release from HUVECs compared to the magnesium alloy. Figures 6C and 6D illustrate the migration of HUVECs in a scratch test and the results of statistical analysis under different culture conditions. The migration rate of HUVECs in the Mg-(SA/CMCS)$_6$ group was faster than that in the Mg substrate group and Control group. After 6 h of

Table 1. Electrochemical parameters of Tafel curves of Mg substrate, Mg-OH and Mg-(SA/CMCS)$_6$ samples in SBF

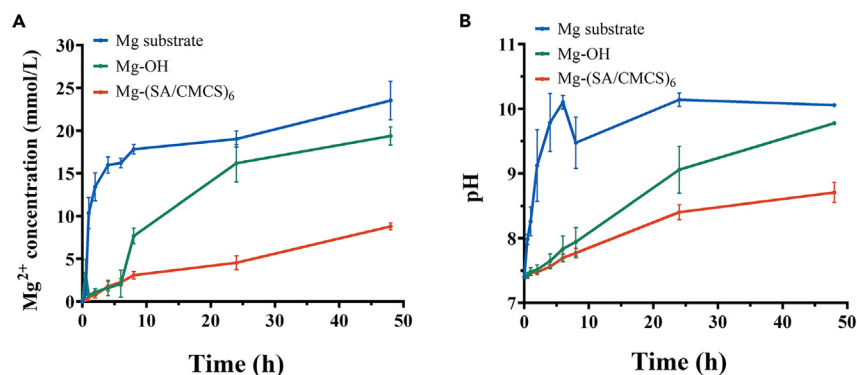| Samples	E$_{corr}$ (V)	i$_{corr}$ (A·cm^{-2})
Mg substrate	−1.732 ± 0.020	(3.187 ± 1.534)×10^{-4}
Mg-OH	−1.512 ± 0.022	(2.284 ± 1.070)×10^{-5}
Mg-(SA/CMCS)$_6$	−1.496 ± 0.009	(2.599 ± 0.675)×10^{-7}

Figure 4. Mg^{2+} and pH of the sample

(A) Mg^{2+} concentration and (B) pH value in the extracts of Mg substrate, Mg-OH and Mg-(SA/CMCS)$_6$ samples after immersion in SBF at 37°C for 0 h, 0.5 h, 1 h, 2 h, 4 h, 6 h, 8 h, 24 h, and 48 h.

scratching, the average cell migration rate of HUVECs in the Mg-(SA/CMCS)$_6$ group was 1.8 times higher than that in the Mg substrate group and 1.2 times higher than that in the Control group. Figures 6E and 6F display the Transwell results and statistical analysis of HUVECs cultured for 24 h. The mean number of cell migration in the Mg-(SA/CMCS)$_6$ group was 1.7 times higher than that in the Mg substrate group and 1.5 times higher than that in the Control group.

To further explore the impact of coating on angiogenesis, angiogenesis experiment was conducted, and the findings are depicted in Figures 6G and 6H. In comparison to the Mg substrate group, the Mg-(SA/CMCS)6 group exhibited a significant increase in the number of nodes within the tubular network. Specifically, the average number of nodes in the Mg-(SA/CMCS)6 group was 2.5 times higher than that in the Mg substrate group, 1.2 times higher than that in the Control group, and 2 times higher than that in the Mg substrate group.

It has been established that the downregulation of von Willebrand Factor (vWF) expression and the upregulation of VE-cadherin expression promote the proliferation and migration of endothelial cells.[46,47] From Figure 7, the elevation of vWF expression and the reduction of VE-cadherin expression in HUVECs from the Mg substrate group were observed. Conversely, the Mg-(SA/CMCS)$_6$ group exhibited decreased vWF expression and increased VE-cadherin expression. Notably, VE-cadherin formed a significant network structure in the Mg-(SA/CMCS)$_6$ group. These results demonstrate that the Mg-(SA/CMCS)$_6$ group promotes the proliferation and migration of HUVECs by regulating the expression of vWF and VE-cadherin.

Effect of coating on smooth muscle cell migration

SMCs are the primary cell type in the pre-atherosclerotic intima, and the influence of coating on the migration of HCASMCs was investigated. HCASMCs were co-cultured with HUVECs, and the results demonstrated that the number of migrating HCASMCs in the Mg-(SA/CMCS)$_6$ group was significantly lower than that in the Mg substrate group (Figure 8). This indicates that the Mg-(SA/CMCS)$_6$ group inhibited SMC migration, while the bare magnesium alloy promoted excessive SMC migration.

Inflammatory response

To understand the effect of coating on inflammation, Arg-1, a marker of M2 macrophages, and factors associated with inflammation, including IL-6, IL-10, ODC-1, TNF-α, Arg-2 were examined, and Netrin-1. Proinflammatory cytokine IL-6 and anti-inflammatory cytokine IL-10 were detected using ELISA. The results revealed that the expression of IL-6 was higher in M0, M1, and M2 macrophages of the magnesium alloy group (Figure 9A), particularly in M1 macrophages. Conversely, the expression of IL-6 in the Mg-(SA/CMCS)$_6$ group
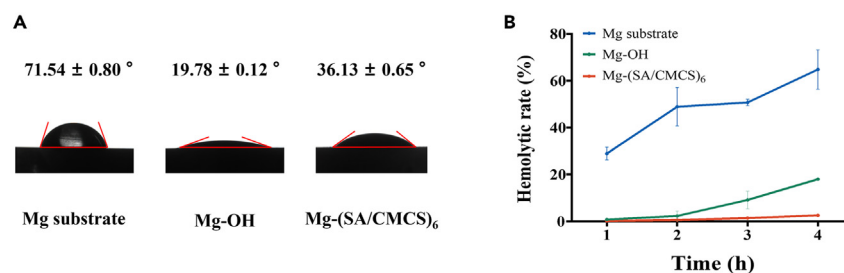

Figure 5. Hydrophobicity and blood compatibility of the sample

(A) Water contact angle of Mg substrate, Mg-OH, and Mg-(SA/CMCS)$_6$ samples; (B) Acute hemolysis test of Mg substrate, Mg-OH, and Mg-(SA/CMCS)$_6$ samples.
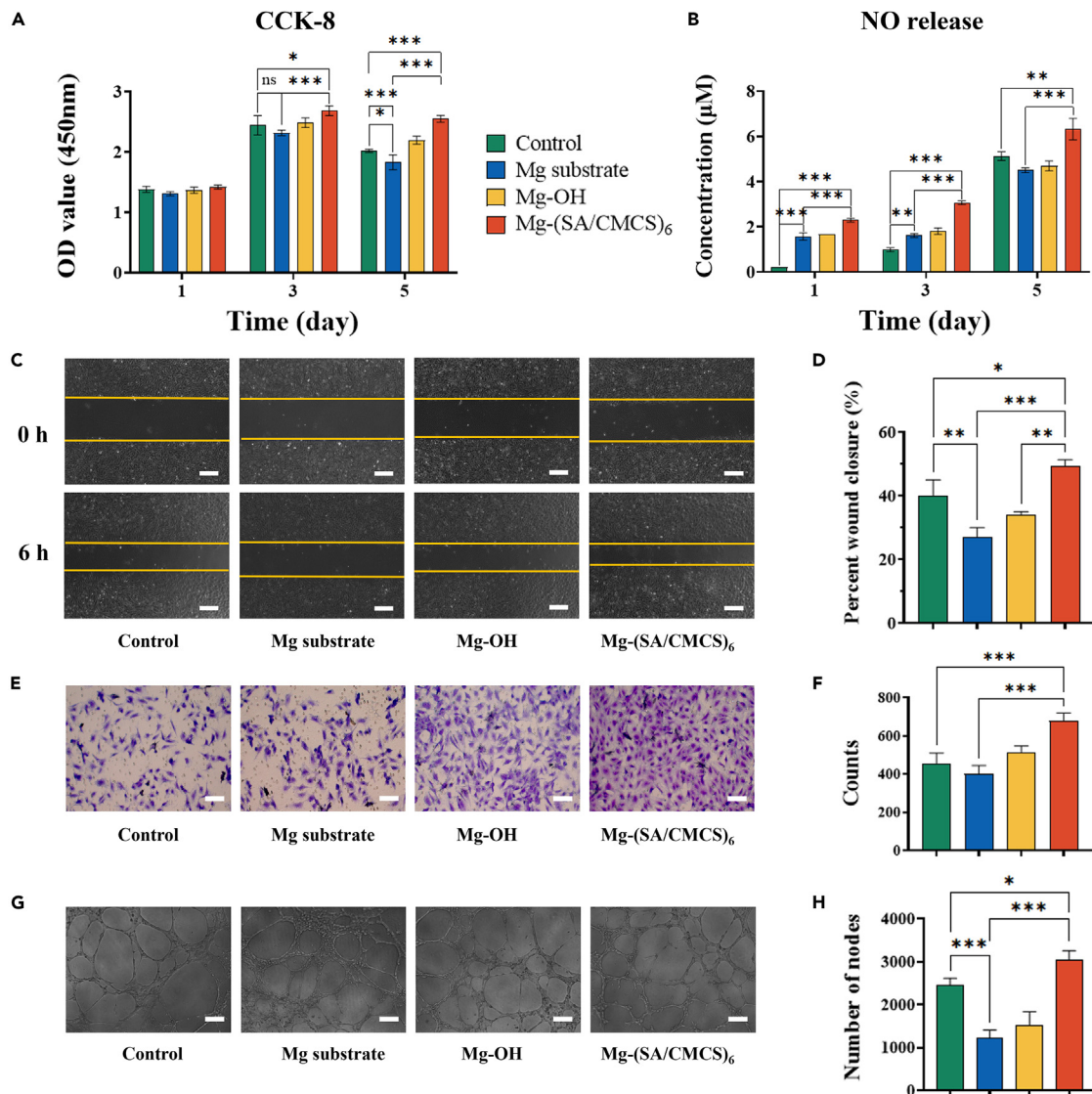
Figure 6. Endothelialization studies of the sample

HUVECs were cultured in Mg substrate, Mg-OH, and Mg-(SA/CMCS)$_6$ medium extracts: (A) CCK-8 was measured after 1 day, 3 days and 5 days of culture; (B) NO release after 1 day, 3 days and 5 days of culture; (C), (D) Migration and quantitative analysis of cells cultured for 0 h and 6 h after scratch (scale bar = 400 μm); (E), (F) Transwell migration and quantitative analysis after 24 h of culture (scale bar = 100 μm); (G), (H) Vascular formation and quantitative analysis after 6 h of culture (scale bar = 200 μm); *p < 0.05, **p < 0.01, ***p < 0.001.

was relatively lower than that in the Control group. There was no significant difference in the expression of the anti-inflammatory cytokine IL-10 (Figure 9B) in M0 macrophages. In the Mg-(SA/CMCS)$_6$ group, IL-10 was highly expressed in M1 and M2 macrophages, with higher expression observed in M2 macrophages. The expression of IL-10 in the Mg-(SA/CMCS)$_6$ group was higher than that in the Control group. The ELISA results indicated that the Mg-(SA/CMCS)$_6$ group promoted the secretion of the anti-inflammatory cytokine IL-10 but had no significant effect on the secretion of the pro-inflammatory cytokine IL-6. The expression of inflammation-related genes in M0 (Figure 9C), M1 (Figure 9D), and M2 (Figure 9E) macrophages was assessed using qRT-PCR. Arg-1 and ODC-1 were upregulated in M0, M1, and M2 macrophages, with higher upregulation observed in the Mg-(SA/CMCS)$_6$ group compared to the Control group. The expression of TNF-α, Arg-2, and Netrin-1 was downregulated, and the downregulation of TNF-α, Arg-2, and Netrin-1 in the Mg-(SA/CMCS)$_6$ group was less pronounced than that in the Control group. These results indicated that SA/CMCS coating could reduce the release of inflammatory factors and dampen the inflammatory response. Furthermore, the SA/CMCS coating group exhibited superior anti-inflammatory properties compared to the control group. Collectively, these findings suggest that the coating attenuates M1 polarization while inducing M2 polarization, thus promoting the production of anti-inflammatory factors and inhibiting the production of pro-inflammatory factors.
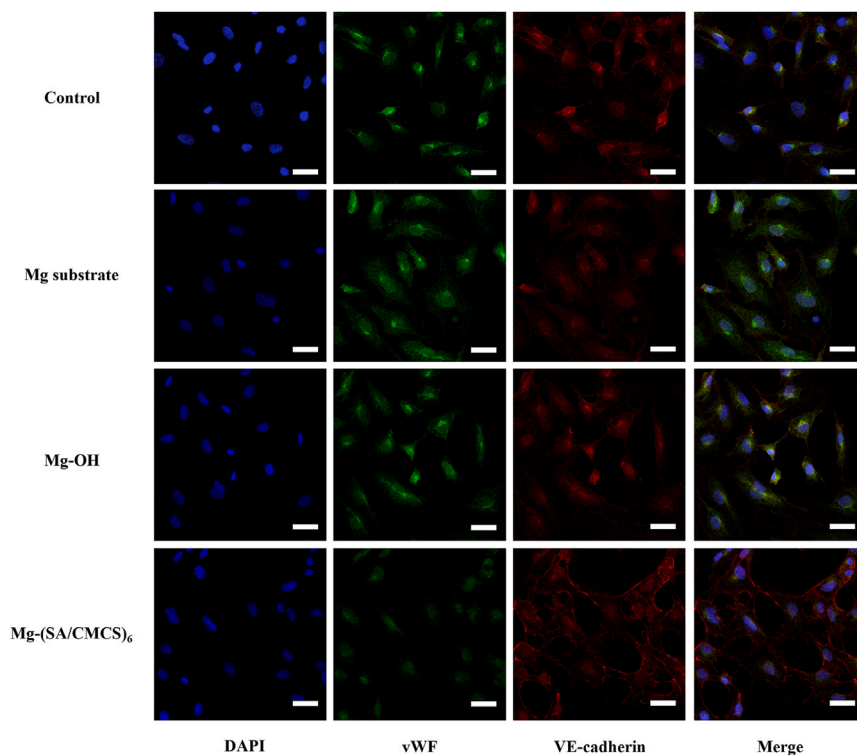
Figure 7. Expression of vWF (green) and VE-cadherin (red) in normal medium and Control, Mg substrate, Mg-OH and Mg-(SA/CMCS)$_6$ extracts (scale bar = 25 μm)

DISCUSSION

In this study, an SA/CMCS multilayer coating was prepared on the surface of the magnesium alloy using the dip coating method. The coating preparation diagram is presented in Figure 10. The hydrothermal treatment resulted in the formation of an Mg(OH)$_2$ layer and SA/CMCS polymer coating was formed on the surface of the magnesium alloy, which served as physical barrier to reduce direct contact between the magnesium alloy substrate and blood. which is because of long-term corrosion protection provided by the synergistic effect of the outer SA/CMCS layer with compact structure and the inner Mg(OH)$_2$ layer. SA[42] and CMCS[33,48] exhibit low cytotoxicity and excellent biocompatibility. SA can form a physical barrier on the surface of magnesium alloy by cross-linking with Ca^{2+} in the blood to create a network structure,[40] thereby reducing direct contact between red blood cells in the blood and the surface of magnesium alloy. Consequently, the hemolysis rate of SA/CMCS sample is significantly lower than 5%, which reduces the likelihood of distal vascular embolism and the risk of cerebral infarction.[49–52]

Magnesium alloy exhibits poor corrosion resistance and limited biological activity prior to surface modification. The presence of Cl$^-$ in body fluids readily corrodes the surface of magnesium alloy, leading to severe corrosion.[53] However, through the layer-by-layer deposition of SA and CMCS in our study, the coating effectively reduces the release of Mg^{2+} and OH$^-$ ions. Maier et al.[54] demonstrated that at appropriate concentration of Mg^{2+} could stimulate the release of more NO from endothelial cells. NO, functioning as an endothelial relaxing factor, plays a crucial role in physiological processes such as promoting endothelial cells growth, inducing vasodilation, and inhibiting SMCs proliferation.[55–57] In our study, the NO release assay revealed that the SA/CMCS coating facilitated increased NO release from endothelial cells, which is essential for endothelial cells growth. It should be noted that NO can inhibit SMCs proliferation. To ascertain whether the NO released by HUVECs can indeed impede the proliferation and migration of SMCs, a co-culture experiment with HUVECs and SMCs were
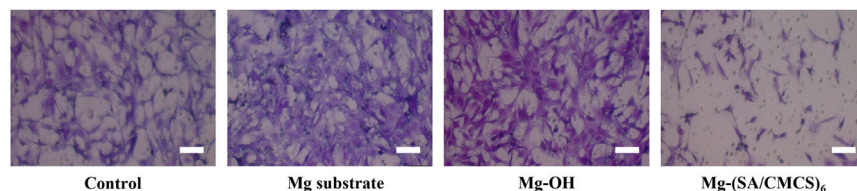

Figure 8. HCASMCs and HUVECs were co-cultured in Control, Mg substrate, Mg-OH and Mg-(SA/CMCS)$_6$ extracts for HCASMCs migration (scale bar = 100 μm)
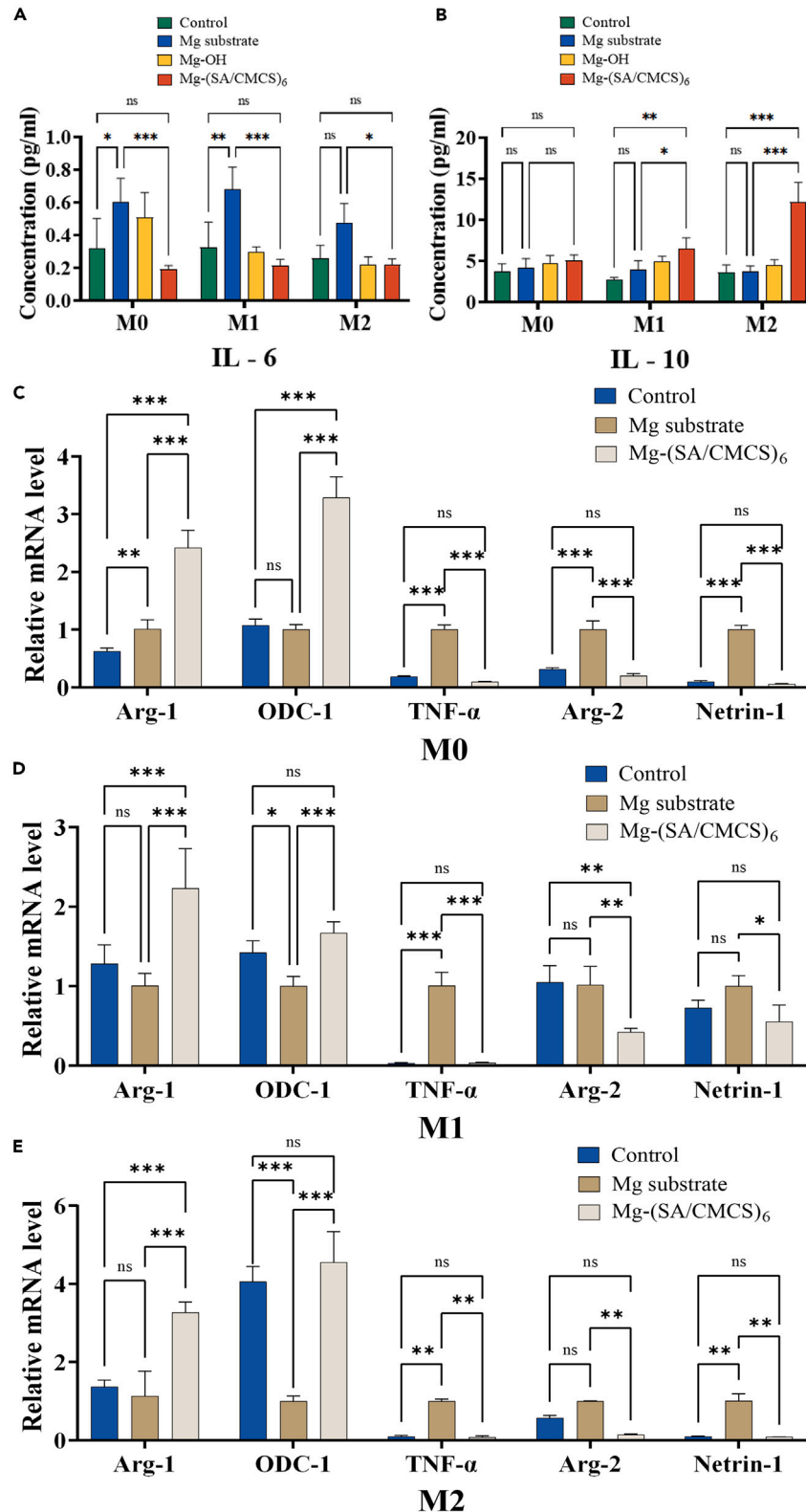
Figure 9. Inflammation studies of the sample

(A), (B) Results of ELISA for IL-6 and IL-10 in M0, M1 and M2 macrophages; (C), (D), (E) qRT-PCR results of relative expression levels of Arg-1, ODC-1, TNF-α, Arg-2 and netin-1 mRNA in M0, M1 and M2 macrophages; *p < 0.05, **p < 0.01, ***p < 0.001.
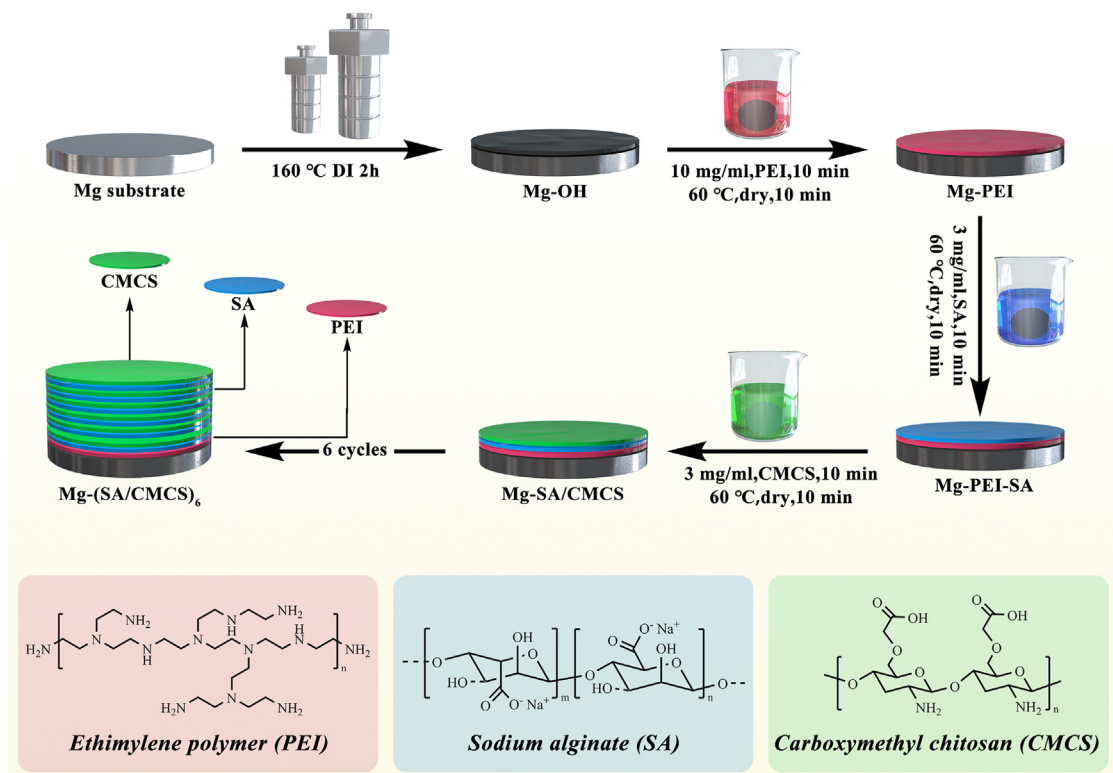
Figure 10. Schematic diagram depicting the preparation of the Mg-(SA/CMCS)₆ composite coating

conducted. The results of the Transwell experiment demonstrated that the number of migrating SMCs in the SA/CMCS group was significantly lower than that in the bare magnesium alloy group. This suggests that the coating effectively restrained the migration of vascular SMCs. It is plausible that the SA/CMCS coating on the magnesium alloy promotes NO release by HUVECs, which, in turn, mediates intercellular communication between HUVECs and SMCs, thus inhibiting the proliferation and migration of SMCs. NO inhibits SMCs migration and proliferation possibly by upregulating cGMP and α-SMA.[55,58] However, further investigation is required to elucidate the precise underlying mechanism.

It has also been demonstrated that the downregulation of vWF expression and the upregulation of VE-cadherin expression promote the proliferation and migration of endothelial cells,[46,47] facilitating the rapid adhesion, proliferation, and migration of endothelial cells on the implant surface, thus promoting the rapid completion of vascularization of stent. In this study, the immunofluorescence assay was employed to verify the expression of two endothelial cells surface markers, vWF and VE-cadherin, which are associated with angiogenesis. The results showed that the expression of vWF was downregulated and VE-cadherin was upregulated in endothelial cells of the SA/CMCS group compared with the Mg substrate group, and VE-cadherin formed a significant reticular formation in SA/CMCS group. These findings indicate that SA/CMCS coating could promote proliferation, migration and angiogenesis of endothelial cells, which is expected to solve the problems of the delayed endothelialization of the implanted Mg-based stent material.

Inflammation and vascular remodeling after stent implantation are highly correlated with local monocyte behavior,[59] and vascular wall injury caused by stent implantation can lead to related inflammation and promote SMCs proliferation, which is the mechanism of in-stent restenosis (ISR). To further understand the effect of the coating on inflammation, relevant inflammatory factors were examined. The coating has been found to promote the secretion of the anti-inflammatory cytokine IL-10 and inhibit the secretion of the pro-inflammatory cytokine IL-6. Increasing evidence shows that the increase of anti-inflammatory M2 macrophages is related to the reduction of ISR,[60,61] reduced inflammatory responses, and increased polarization of M2 macrophages with the ability to undergo rapid endothelialization and promotes angiogenesis. Moreover, the SA/CMCS coating effectively hinders SMCs migration and exhibits anti-inflammatory properties. Therefore, the SA/CMCS coating is expected to be an ideal coating for biodegradable magnesium alloy vascular stent (Figure 11).

Conclusions

In this work, a biodegradable SA/CMCS coating was successfully constructed on the surface of ZE21B magnesium alloy via hydrothermal treatment and dipping treatments, and the main conclusions of this study are the following.
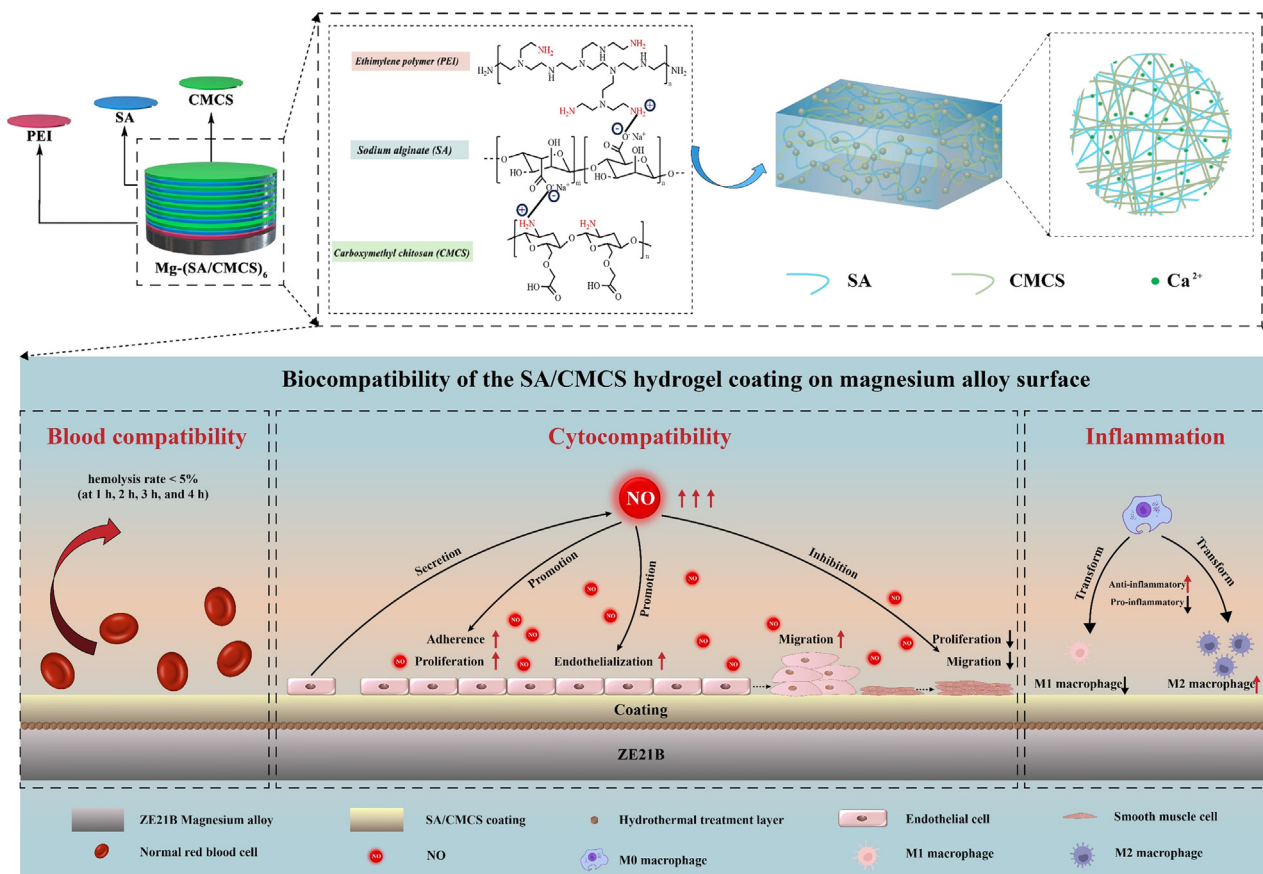
Figure 11. Mechanism of SA/CMCS coating on the biocompatibility of the surface of magnesium alloy

1) The SA/CMCS coating sample shows a low degradation rate, which will be beneficial to improve the biocompatibility of the surface of magnesium alloy.
2) The hemocompatibility tests indicate that the SA/CMCS coating exhibits a lower hemolysis rate, confirming its better anti-hemolysis properties and blood compatibility.
3) The NO release assay demonstrates that the SA/CMCS coating promotes NO release from HUVECs more effectively compared to the Mg substrate.
4) Cytocompatibility assay shows that the SA/CMCS coating facilitates the growth, proliferation, and migration of endothelial cells and promotes neovascularization.
5) The SA/CMCS coating effectively reduces M1 polarization and promotes M2 polarization, resulting in increased production of anti-inflammatory molecules and suppression of pro-inflammatory molecules in the inflammatory response.

Limitations of the study

The limitation of this study is that no animal model was used to validate the coated magnesium alloys. We hope that animal models can be used in subsequent studies to verify the corrosion resistance and biocompatibility of magnesium alloys after coating.

STAR★METHODS

Detailed methods are provided in the online version of this paper and include the following:

- KEY RESOURCES TABLE
- RESOURCE AVAILABILITY
  - Lead contact
  - Materials availability
  - Data and code availability
- EXPERIMENTAL MODEL AND STUDY PARTICIPANT DETAILS

○ Cell lines
● METHOD DETAILS
  ○ Coating preparation
  ○ Characterization of coating surface structure and properties
  ○ Cytocompatibility
  ○ *In vitro* culture of HCASMCs
  ○ *In vitro* culture of THP-1
● QUANTIFICATION AND STATISTICAL ANALYSIS

SUPPLEMENTAL INFORMATION

Supplemental information can be found online at https://doi.org/10.1016/j.isci.2024.109197.

AUTHOR CONTRIBUTIONS

Conceptualization: R.J.; Formal analysis: R.J., Investigation: R.J. and Y.H.; Writing - Original Draft: R.J., Y.H., and J.L.; Visualization: R.J. and J.L.; Data curation: R.J., Y.H., J.L., L.D., C.M., T.L., W.L., and S.L.; Methodology: H.W. and H.C.; Resources: H.W. and H.C.; Funding acquisition: T.L. and Y.H; Supervision: T.L. and Y.H; Writing – Review and Editing: T.L. and Y.H.; Project administration: T.L. and Y.H. All authors read and approved the final manuscript.

DECLARATION OF INTERESTS

The authors declare no competing interests.

REFERENCES

1. Qureshi, A.I., and Caplan, L.R. (2014). Intracranial atherosclerosis. Lancet *383*, 984–998. https://doi.org/10.1016/S0140-6736(13)61088-0.

2. Park, H., Baek, J.-H., and Kim, B.M. (2019). Endovascular Treatment of Acute Stroke Due to Intracranial Atherosclerotic Stenosis-Related Large Vessel Occlusion. Front. Neurol. *10*, 308. https://doi.org/10.3389/fneur.2019.00308.

3. van den Wijngaard, I.R., Holswilder, G., van Walderveen, M.A.A., Algra, A., Wermer, M.J.H., Zaidat, O.O., and Boiten, J. (2016). Treatment and imaging of intracranial atherosclerotic stenosis: current perspectives and future directions. Brain Behav. *6*, e00536. https://doi.org/10.1002/brb3.536.

4. Wang, S., Zhang, X., Li, J., Liu, C., and Guan, S. (2020). Investigation of Mg-Zn-Y-Nd alloy for potential application of biodegradable esophageal stent material. Bioact. Mater. *5*, 1–8. https://doi.org/10.1016/j.bioactmat.2020.01.002.

5. Liu, M., Wang, J., Zhu, S., Zhang, Y., Sun, Y., Wang, L., and Guan, S. (2020). Corrosion fatigue of the extruded Mg–Zn–Y–Nd alloy in simulated body fluid. J. Magnesium Alloys *8*, 231–240. https://doi.org/10.1016/j.jma.2019.09.009.

6. Wang, H., Yuan, H., Wang, J., Zhang, E., Bai, M., Sun, Y., Wang, J., Zhu, S., Zheng, Y., and Guan, S. (2021). Influence of the second phase on protein adsorption on biodegradable Mg alloys' surfaces: Comparative experimental and molecular dynamics simulation studies. Acta Biomater. *129*, 323–332. https://doi.org/10.1016/j.actbio.2021.03.063.

7. Liu, C., Chen, L., Zhang, K., Li, J., and Guan, S. (2022). Tailoring ZE21B Alloy with Nature-Inspired Extracellular Matrix Secreted by Micro-Patterned Smooth Muscle Cells and Endothelial Cells to Promote Surface Biocompatibility. IJMS *23*, 3180. https://doi.org/10.3390/ijms23063180.

8. Li, W., Su, Y., Ma, L., Zhu, S., Zheng, Y., and Guan, S. (2021). Sol-gel coating loaded with inhibitor on ZE21B Mg alloy for improving corrosion resistance and endothelialization aiming at potential cardiovascular application. Colloids Surf. B Biointerfaces *207*, 111993. https://doi.org/10.1016/j.colsurfb.2021.111993.

9. Feng, H., Liu, H., Cao, H., Yang, Y., Xu, Y., and Guan, J. (2015). Effect of precipitates on mechanical and damping properties of Mg–Zn–Y–Nd alloys. Mater. Sci. Eng. *639*, 1–7. https://doi.org/10.1016/j.msea.2015.04.092.

10. Hou, S.S., Zhang, R.R., Guan, S.K., Ren, C.X., Gao, J.H., Lu, Q.B., and Cui, X.Z. (2012). In vitro corrosion behavior of Ti-O film deposited on fluoride-treated Mg–Zn–Y–Nd alloy. Appl. Surf. Sci. *258*, 3571–3577. https://doi.org/10.1016/j.apsusc.2011.11.116.

11. Haude, M., Ince, H., Abizaid, A., Toelg, R., Lemos, P.A., Von Birgelen, C., Christiansen, E.H., Wijns, W., Neumann, F.-J., Kaiser, C., et al. (2016). Safety and performance of the second-generation drug-eluting absorbable metal scaffold in patients with de-novo coronary artery lesions (BIOSOLVE-II): 6 month results of a prospective, multicentre, non-randomised, first-in-man trial. Lancet *387*, 31–39. https://doi.org/10.1016/S0140-6736(15)00447-X.

12. Witte, F. (2010). The history of biodegradable magnesium implants: a review. Acta Biomater. *6*, 1680–1692. https://doi.org/10.1016/j.actbio.2010.02.028.

13. Bommala, V.K., Krishna, M.G., and Rao, C.T. (2019). Magnesium matrix composites for biomedical applications: A review. J. Magnesium Alloys *7*, 72–79. https://doi.org/10.1016/j.jma.2018.11.001.

14. Zhang, Z.-Q., Yang, Y.-X., Li, J.-A., Zeng, R.-C., and Guan, S.-K. (2021). Advances in coatings on magnesium alloys for cardiovascular stents – A review. Bioact. Mater. *6*, 4729–4757. https://doi.org/10.1016/j.bioactmat.2021.04.044.

15. Esmaily, M., Svensson, J.E., Fajardo, S., Birbilis, N., Frankel, G.S., Virtanen, S., Arrabal, R., Thomas, S., and Johansson, L.G. (2017).

Fundamentals and advances in magnesium alloy corrosion. Prog. Mater. Sci. *89*, 92–193. https://doi.org/10.1016/j.pmatsci.2017.04.011.

16. Ma, C., Peng, G., Nie, L., Liu, H., and Guan, Y. (2018). Laser surface modification of Mg-Gd-Ca alloy for corrosion resistance and biocompatibility enhancement. Appl. Surf. Sci. *445*, 211–216. https://doi.org/10.1016/j.apsusc.2018.03.174.

17. Xue, K., Tan, P.-H., Zhao, Z.-H., Cui, L.-Y., Kannan, M.B., Li, S.-Q., Liu, C.-B., Zou, Y.-H., Zhang, F., Chen, Z.-Y., and Zeng, R.C. (2023). In vitro degradation and multi-antibacterial mechanisms of β-cyclodextrin@curcumin embodied Mg(OH)2/MAO coating on AZ31 magnesium alloy. J. Mater. Sci. Technol. *132*, 179–192. https://doi.org/10.1016/j.jmst.2022.04.053.

18. Zhang, A.-M., Lenin, P., Zeng, R.-C., and Kannan, M.B. (2022). Advances in hydroxyapatite coatings on biodegradable magnesium and its alloys. J. Magnesium Alloys *10*, 1154–1170. https://doi.org/10.1016/j.jma.2022.01.001.

19. Zhang, Z.-Y., An, Y.-L., Wang, X.-S., Cui, L.-Y., Li, S.-Q., Liu, C.-B., Zou, Y.-H., Zhang, F., and Zeng, R.-C. (2022). In vitro degradation, photo-dynamic and thermal antibacterial activities of Cu-bearing chlorophyllin-induced Ca–P coating on magnesium alloy AZ31. Bioact. Mater. *18*, 284–299. https://doi.org/10.1016/j.bioactmat.2022.01.050.

20. Zhang, G., Jiang, E., Wu, L., Tang, A., Atrens, A., and Pan, F. (2022). Active corrosion protection of phosphate loaded PEO/LDHs composite coatings: SIET study. J. Magnesium Alloys *10*, 1351–1357. https://doi.org/10.1016/j.jma.2021.03.008.

21. Córdoba, L.C., Hélary, C., Montemor, F., and Coradin, T. (2019). Bi-layered silane-TiO2/collagen coating to control biodegradation and biointegration of Mg alloys. Mater. Sci. Eng., C *94*, 126–138. https://doi.org/10.1016/j.msec.2018.09.032.

22. Córdoba, L.C., Marques, A., Taryba, M., Coradin, T., and Montemor, F. (2018). Hybrid coatings with collagen and chitosan for improved bioactivity of Mg alloys. Surf. Coating. Technol. *341*, 103–113. https://doi.org/10.1016/j.surfcoat.2017.08.062.

23. Bakhsheshi-Rad, H.R., Chen, X., Ismail, A.F., Aziz, M., Abdolahi, E., and Mahmoodiyan, F. (2019). Improved antibacterial properties of an Mg-Zn-Ca alloy coated with chitosan nanofibers incorporating silver sulfadiazine multiwall carbon nanotubes for bone implants. Polym. Adv. Technol. *30*, 1333–1339. https://doi.org/10.1002/pat.4563.

24. Cui, L.-Y., Gao, L., Zhang, J.-C., Tang, Z., Fan, X.-L., Liu, J.-C., Chen, D.-C., Zeng, R.-C., Li, S.-Q., and Zhi, K.-Q. (2021). In vitro corrosion resistance, antibacterial activity and cytocompatibility of a layer-by-layer assembled DNA coating on magnesium alloy. J. Magnesium Alloys *9*, 266–280. https://doi.org/10.1016/j.jma.2020.03.009.

25. Sangeetha, K., Roy, A., Singh, S., Lee, B., and Kumta, P.N. (2011). Novel alginate based coatings on Mg alloys. Mater. Sci. Eng., B *176*, 1703–1710. https://doi.org/10.1016/j.mseb.2011.08.004.

26. Zou, Q., Grottkau, B.E., He, Z., Shu, L., Yang, L., Ma, M., and Ye, C. (2020). Biofabrication of valentine-shaped heart with a composite hydrogel and sacrificial material. Mater. Sci. Eng., C *108*, 110205. https://doi.org/10.1016/j.msec.2019.110205.

27. Li, L.-Y., Cui, L.-Y., Zeng, R.-C., Li, S.-Q., Chen, X.-B., Zheng, Y., and Kannan, M.B. (2018). Advances in functionalized polymer coatings on biodegradable magnesium alloys – A review. Acta Biomater. *79*, 23–36. https://doi.org/10.1016/j.actbio.2018.08.030.

28. Agarwal, S., Morshed, M., Labour, M.-N., Hoey, D., Duffy, B., Curtin, J., and Jaiswal, S. (2016). Enhanced corrosion protection and biocompatibility of a PLGA–silane coating on AZ31 Mg alloy for orthopaedic applications. RSC Adv. *6*, 113871–113883. https://doi.org/10.1039/c6ra24382g.

29. Younes, I., and Rinaudo, M. (2015). Chitin and chitosan preparation from marine sources. Structure, properties and applications. Mar. Drugs *13*, 1133–1174. https://doi.org/10.3390/md13031133.

30. Zhang, Y., Zhao, W., Lin, Z., Tang, Z., and Lin, B. (2023). Carboxymethyl chitosan/sodium alginate hydrogel films with good biocompatibility and reproducibility by in situ ultra-fast crosslinking for efficient preservation of strawberry. Carbohydr. Polym. *316*, 121073. https://doi.org/10.1016/j.carbpol.2023.121073.

31. Salama, A., Mohamed, F., and Hesemann, P. (2022). Dielectric properties of chitosan and two ionic derivatives: Effect of counter anions. Carbohydr. Polym. *297*, 120018. https://doi.org/10.1016/j.carbpol.2022.120018.

32. Zhang, J., Wang, L., Tan, W., Li, Q., Dong, F., and Guo, Z. (2022). Preparation of chitosan-rosmarinic acid derivatives with enhanced antioxidant and anti-inflammatory activities. Carbohydr. Polym. *296*, 119943. https://doi.org/10.1016/j.carbpol.2022.119943.

33. Vaz, J.M., Taketa, T.B., Hernandez-Montelongo, J., Chevallier, P., Cotta, M.A., Mantovani, D., and Beppu, M.M. (2018). Antibacterial properties of chitosan-based coatings are affected by spacer-length and molecular weight. Appl. Surf. Sci. *445*, 478–487. https://doi.org/10.1016/j.apsusc.2018.03.110.

34. Arima, Y., and Iwata, H. (2007). Effect of wettability and surface functional groups on protein adsorption and cell adhesion using well-defined mixed self-assembled monolayers. Biomaterials *28*, 3074–3082. https://doi.org/10.1016/j.biomaterials.2007.03.013.

35. Li, Y., Shan, P., Yu, F., Li, H., and Peng, L. (2023). Fabrication and characterization of waste fish scale-derived gelatin/sodium alginate/carvacrol loaded ZIF-8 nanoparticles composite films with sustained antibacterial activity for active food packaging. Int. J. Biol. Macromol. *230*, 123192. https://doi.org/10.1016/j.ijbiomac.2023.123192.

36. Şen, F., Uzunsoy, İ., Baştürk, E., and Kahraman, M.V. (2017). Antimicrobial agent-free hybrid cationic starch/sodium alginate polyelectrolyte films for food packaging materials. Carbohydr. Polym. *170*, 264–270. https://doi.org/10.1016/j.carbpol.2017.04.079.

37. Sun, J.-Y., Zhao, X., Illeperuma, W.R.K., Chaudhuri, O., Oh, K.H., Mooney, D.J., Vlassak, J.J., and Suo, Z. (2012). Highly stretchable and tough hydrogels. Nature *489*, 133–136. https://doi.org/10.1038/nature11409.

38. Gao, C., Liu, M., Chen, S., Jin, S., and Chen, J. (2009). Preparation of oxidized sodium alginate-graft-poly((2-dimethylamino) ethyl methacrylate) gel beads and in vitro controlled release behavior of BSA. Int. J.

Pharm. *371*, 16–24. https://doi.org/10.1016/j.ijpharm.2008.12.013.

39. Gao, C., Liu, M., Chen, J., and Zhang, X. (2009). Preparation and controlled degradation of oxidized sodium alginate hydrogel. Polym. Degrad. Stabil. *94*, 1405–1410. https://doi.org/10.1016/j.polymdegradstab.2009.05.011.

40. Liu, H., Wang, C., Gao, Q., Chen, J., Ren, B., Liu, X., and Tong, Z. (2009). Facile fabrication of well-defined hydrogel beads with magnetic nanocomposite shells. Int. J. Pharm. *376*, 92–98. https://doi.org/10.1016/j.ijpharm.2009.04.031.

41. Lee, K.Y., and Mooney, D.J. (2012). Alginate: Properties and biomedical applications. Prog. Polym. Sci. *37*, 106–126. https://doi.org/10.1016/j.progpolymsci.2011.06.003.

42. Lan, S.-F., Safiejko-Mroczka, B., and Starly, B. (2010). Long-term cultivation of HepG2 liver cells encapsulated in alginate hydrogels: a study of cell viability, morphology and drug metabolism. Toxicol. Vitro *24*, 1314–1323. https://doi.org/10.1016/j.tiv.2010.02.015.

43. Grassi, M., Colombo1, I., and Lapasin, R. (2000). Drug release from an ensemble of swellable crosslinked polymer particles. J. Contr. Release *68*, 97–113. https://doi.org/10.1016/s0168-3659(00)00241-8.

44. Wawrzyńska, E., and Kubies, D. (2018). Alginate matrices for protein delivery - a short review. Physiol. Res. *67*, S319–S334. https://doi.org/10.33549/physiolres.933980.

45. Blandino, A., Macías, M., and Cantero, D. (2000). Glucose oxidase release from calcium alginate gel capsules. Enzym. Microb. Technol. *27*, 319–324. https://doi.org/10.1016/s0141-0229(00)00204-0.

46. Starke, R.D., Ferraro, F., Paschalaki, K.E., Dryden, N.H., McKinnon, T.A.J., Sutton, R.E., Payne, E.M., Haskard, D.O., Hughes, A.D., Cutler, D.F., et al. (2011). Endothelial von Willebrand factor regulates angiogenesis. Blood *117*, 1071–1080. https://doi.org/10.1182/blood-2010-01-264507.

47. McEvoy, E., Sneh, T., Moeendarbary, E., Javanmardi, Y., Efimova, N., Yang, C., Marino-Bravante, G.E., Chen, X., Escribano, J., Spill, F., et al. (2022). Feedback between mechanosensitive signaling and active forces governs endothelial junction integrity. Nat. Commun. *13*, 7089. https://doi.org/10.1038/s41467-022-34701-y.

48. Kerec, M., Bogataj, M., Veranic, P., and Mrhar, A. (2005). Permeability of pig urinary bladder wall: the effect of chitosan and the role of calcium. Eur. J. Pharmaceut. Sci. *25*, 113–121. https://doi.org/10.1016/j.ejps.2005.02.003.

49. Zhu, Y., Zhang, H., Zhang, Y., Wu, H., Wei, L., Zhou, G., Zhang, Y., Deng, L., Cheng, Y., Li, M., et al. (2019). Endovascular Metal Devices for the Treatment of Cerebrovascular Diseases. Adv. Mater. *31*, e1805452. https://doi.org/10.1002/adma.201805452.

50. Zhao, W., Kong, M., Feng, C., Cheng, X., Liu, Y., and Chen, X. (2016). Investigation of gelling behavior of thiolated chitosan in alkaline condition and its application in stent coating. Carbohydr. Polym. *136*, 307–315. https://doi.org/10.1016/j.carbpol.2015.09.049.

51. Wang, J.l., Li, B.c., Li, Z.j., Ren, K.f., Jin, L.j., Zhang, S.m., Chang, H., Sun, Y.x., and Ji, J. (2014). Electropolymerization of dopamine for surface modification of complex-shaped cardiovascular stents. Biomaterials *35*, 7679–7689. https://doi.org/10.1016/j.biomaterials.2014.05.047.

52. Denardo, S.J., Carpinone, P.L., Vock, D.M., Batich, C.D., and Pepine, C.J. (2012). Changes to polymer surface of drug-eluting stents during balloon expansion. JAMA *307*, 2148–2150. https://doi.org/10.1001/jama.2012.4111.

53. Gao, F., Hu, Y., Li, G., Liu, S., Quan, L., Yang, Z., Wei, Y., and Pan, C. (2020). Layer-by-layer deposition of bioactive layers on magnesium alloy stent materials to improve corrosion resistance and biocompatibility. Bioact. Mater. *5*, 611–623. https://doi.org/10.1016/j.bioactmat.2020.04.016.

54. Maier, J.A.M., Bernardini, D., Rayssiguier, Y., and Mazur, A. (2004). High concentrations of magnesium modulate vascular endothelial cell behaviour *in vitro*. Biochim. Biophys. Acta *1689*, 6–12. https://doi.org/10.1016/j.bbadis.2004.02.004.

55. Qiu, H., Qi, P., Liu, J., Yang, Y., Tan, X., Xiao, Y., Maitz, M.F., Huang, N., and Yang, Z. (2019). Biomimetic engineering endothelium-like coating on cardiovascular stent through heparin and nitric oxide-generating compound synergistic modification strategy. Biomaterials *207*, 10–22. https://doi.org/10.1016/j.biomaterials.2019.03.033.

56. Yang, Z., Yang, Y., Zhang, L., Xiong, K., Li, X., Zhang, F., Wang, J., Zhao, X., and Huang, N. (2018). Mussel-inspired catalytic selenocystamine-dopamine coatings for long-term generation of therapeutic gas on cardiovascular stents. Biomaterials *178*, 1–10. https://doi.org/10.1016/j.biomaterials.2018.06.008.

57. Fan, Y., Zhang, Y., Zhao, Q., Xie, Y., Luo, R., Yang, P., and Weng, Y. (2019). Immobilization of nano Cu-MOFs with polydopamine coating for adaptable gasotransmitter generation and copper ion delivery on cardiovascular stents. Biomaterials *204*, 36–45. https://doi.org/10.1016/j.biomaterials.2019.03.007.

58. Beamish, J.A., Geyer, L.C., Haq-Siddiqi, N.A., Kottke-Marchant, K., and Marchant, R.E. (2009). The effects of heparin releasing hydrogels on vascular smooth muscle cell phenotype. Biomaterials *30*, 6286–6294. https://doi.org/10.1016/j.biomaterials.2009.08.004.

59. Hu, S., Li, Z., Shen, D., Zhu, D., Huang, K., Su, T., Dinh, P.-U., Cores, J., and Cheng, K. (2021). Exosome-eluting stents for vascular healing after ischaemic injury. Nat. Biomed. Eng. *5*, 1174–1188. https://doi.org/10.1038/s41551-021-00705-0.

60. Stark, K., and Massberg, S. (2021). Interplay between inflammation and thrombosis in cardiovascular pathology. Nat. Rev. Cardiol. *18*, 666–682. https://doi.org/10.1038/s41569-021-00552-1.

61. Yan, W., Li, T., Yin, T., Hou, Z., Qu, K., Wang, N., Durkan, C., Dong, L., Qiu, J., Gregersen, H., and Wang, G. (2020). M2 macrophage-derived exosomes promote the c-KIT phenotype of vascular smooth muscle cells during vascular tissue repair after intravascular stent implantation. Theranostics *10*, 10712–10728. https://doi.org/10.7150/thno.46143.

STAR★METHODS

KEY RESOURCES TABLE

REAGENT or RESOURCE	SOURCE	IDENTIFIER
Antibodies		
Anti-vWF antibody	Abcam	RRID: AB_3094475
Anti-VE-cadherin antibody	Proteintech	RRID: AB_2920043
Alexa Fluor®488	Abcam	RRID: AB_2630356
Alexa Fluor®647	Abcam	RRID: AB_2687948
Chemicals, peptides, and recombinant proteins		
Sodium alginate(SA)	Aladdin	S278630
Carboxymethyl chitosan(CMCS, MW=240Kda)	Macklin	C914893
Ethylene imine polymer (PEI, MW=600, 99%)	Macklin	E808878
Matrigel	ABW	0827065
Fluorescent mounting medium (containing DAPI)	ORIGENE	ZU-9557
Cell Counting Kit-8	Meilun Biotechnology Co., Ltd	MA0218-5
Crystal Violet-Gentian Violet Stain Solution	Solarbio	G1075
Software and algorithms		
Image J	NIH	N/A
GraphPad Prism 9.0.0	GraphPad	N/A
Origin	Origin Lab	N/A
CHI 760E	CHI Instruments	N/A

RESOURCE AVAILABILITY

Lead contact

Further information and requests for resources and reagents should be directed to and will be fulfilled by the lead contact, Yingkun He (heyingkun@zzu.edu.cn).

Materials availability

All materials are from commercial sources and are widely available.

Data and code availability

Original data are available from corresponding authors.
  This paper does not report the original code.
  Any additional information required to reanalyze the data reported in this paper is available from the lead contact upon request.

EXPERIMENTAL MODEL AND STUDY PARTICIPANT DETAILS

Cell lines

HUVECs (PCS-100-010, ATCC, USA) were used and cultured in an incubator at 37°C and 5% CO_2. The medium used consisted of 500 ml of ECM, 25 ml of FBS, 5 ml of P/S, and 5 ml of ECGS (1001, Sciencell, USA). When the cells reached 75% to 80% confluence in the culture flask, they were collected for the subsequent experiment.

  HCASMCs (HTX2054, OTWO BIO, China) were used and cultured in an incubator at 37°C and 5% CO_2. The medium used consisted of 500 ml of SMCM, 25 ml of FBS, 5 ml of P/S, and 5 ml of SMCGS (1101, Sciencell, USA).

  THP-1 (341989, BNCC, China) cells were cultured in a cell incubator at 37°C with 5% CO_2. RPMI-1640 complete medium (338360, BNCC, China) was used to culture the cells.

METHOD DETAILS

Coating preparation

The ZE21B magnesium alloy was cut into a cylinder with a height of 3 mm and a diameter of 10 mm. The magnesium alloy samples underwent a surface preparation procedure involving sequential sanding with silicon carbide waterproof papers of 400#, 800#, 1200#, and 4000# grit sizes.Subsequently, the samples were polished using PCY wool fabric polishing cloth with QMOVE diamond suspension polishing liquid (3μm, DS001-C, TRUER) and PCV flannelette (red short velvet) polishing cloth with QMOVE diamond suspension polishing liquid (0.5μm, DS001-C, TRUER). To ensure optimal surface cleanliness, the polished magnesium alloy samples were subjected to ultrasonic cleaning in acetone for 10 minutes and in absolute ethyl alcohol for 10 minutes, effectively eliminating any stains and grease residues. Next, the cleaned Mg substrate was dried in warm air for standby.

The polished magnesium alloy sheets were placed in a Teflon-lined stainless steel autoclave and subjected to hydrothermal treatment at 160°C for 2 hours. and solution C, consisting of a 3 mg/ml CMCS solution, were prepared. Three solution have been prepared, namely solution A, B, C. Solution A is prepared by adding PEI to ultrapure water (Milli-Q Reference, Millipore, USA), which resulted a final concentration of 10 mg/mL. Solution B is prepared by adding SA to ultrapure water, which resulted a final concentration of 3 mg/mL. Solution C is prepared by adding CMCS to ultrapure water, which resulted a final concentration of 3 mg/mL.

Firstly, the pretreated magnesium alloy sheet was immersed in solution A for 10 minutes and then dried in an electrothermal blast drying oven at 37°C for 10 minutes, resulting in the formation of a PEI polymer film on the magnesium alloy surface. This sample was denoted as Mg-PEI. Subsequently, the sample was immersed in solution B for 10 minutes, followed by drying at 37°C for 10 minutes, resulting in the formation of a SA coating, and this sample was denoted as Mg-SA. Next, the sample was immersed in solution C for 10 minutes and dried at 37°C for 10 minutes, resulting in the formation of a CMCS coating, and this sample was denoted as Mg-SA/CMCS. This process of immersion in solutions B and C was repeated five times, with the coating sequence being "ABCBCBCBCBCBC". Finally, after drying, the fully coated sample was obtained and designated as Mg-(SA/CMCS)$_6$. The coating preparation diagram is presented in Figure 10.

Characterization of coating surface structure and properties

Coating surface structure characterization

Scanning electron microscopy (SEM, JSM-7800F, Japan) at an acceleration voltage of 5 kV was employed to characterize the surface topography of the samples both before and after coating. Atomic force microscopy (AFM, Bruker Dimension Icon, Germany) was utilized to examine the surface topography and roughness of the samples with tapping model. X-ray photoelectron spectroscopy (XPS, Thermo Scientific K-Alpha, USA) was employed to detect the elements present on each layer of the samples with an energy resolution of 100 eV wide spectrum and 50 eV narrow spectrum, and the data were analyzed using Avantage software. The surface phase analysis of the samples were analyzed using an X-ray diffractometer (XRD, Bruker D8 Advance, Germany) with copper target (λ = 0.154 nm), a voltage of 40 kV and a current of 40 mA. The data were analyzed using MDI Jade 6 software.

Scratch measurement

Scratch measurements were implemented to represent the adhesion force of the coating (critical load) via Micro combination tester: MCT3 (Anton Paar, Austria). Scratches of 2 mm length were made by a diamond Rockwell indenter with a spherical tip radius of 50 μm sliding at a constant speed of 2 mm/min under increasing loads from 0.01 to 3 N. The tests were repeated for three times.

Electrochemical testing

The Tafel curves of the Mg substrate, Mg-OH, and Mg-(SA/CMCS)$_6$ samples were measured using an electrochemical workstation (CHI760E, Chenhua, China). Prior to obtaining the Tafel curve, the open-circuit voltage of the sample was measured after leaving it to stand for 1 hour, following which the Tafel curve was obtained. The experiment employed a three-electrode mode, with the counter electrode, reference electrode, and working electrode being a platinum electrode (260), a saturated calomel electrode, and the sample to be tested, respectively. The polarization voltage scanning range was set from -2.3 V to -0.9 V, and a scanning speed of 0.01 V/s was employed to measure the open circuit potential and Tafel curve. The Tafel extrapolation method was used to fit the curve, allowing for the determination of the corrosion potential and corrosion current.

Mg^{2+} concentration and pH value

Mg substrate, Mg-OH, and Mg-(SA/CMCS)$_6$ samples were prepared for the detection of Mg^{2+} concentration and pH value in the *in vitro* immersion test. The alloy sheet samples were placed into the 24-well plates with 1 piece per well, and 4 duplicate wells were set up in each group. Simulated body fluid (SBF) (composition provided in Table S1) was added to each well at a volume of 2 ml per well, followed by placing the plates in a 37°C oven. The soaking solution was collected at 0 h, 0.5 h, 1 h, 2 h, 4 h, 6 h, 8 h, 24 h, and 48 h. The absorbance value (OD value) of each sample group were measured at 540 nm using a microplate reader with the aid of an Mg^{2+} detection kit (E-BC-K162-M, Elabscience, China) in order to calculate the Mg^{2+} concentration. The pH value of the soaking solution was determined using a pH meter (PB-10, Sartorlus, Germany). Four samples were measured and the average value was calculated.

Hydrophilic test

A sessile drop of 16 μL of ultra-pure water was placed on the surface, and the contact angle was measured using a contact angle measuring instrument (JY-82C, Chengde Dingsheng, China). The surface hydrophilicity properties of the samples before and after coating were assessed. At least four contact angles were measured in different areas of the sample, and the average value was calculated.

Hemolysis rate

EDTA anticoagulant tubes were obtained from ICAS patient blood, the red blood cells were obtained after being centrifugated at 1500 g and 4°C with a high-speed refrigerated centrifuge (Thermo Heraeus Megafuge 8R, USA) for 10 min. The samples were soaked in 3 ml of a 1% red blood cells solution (diluted in normal saline). Additionally, a negative control group consisting of 1% red blood cells (diluted in normal saline) and a positive control group consisting of 1% red blood cells (diluted in distilled water) were set up. The samples were incubated at 37°C for 1 h, 2 h, 3 h, and 4 h, followed by centrifugation at 3000 rpm for 5 min. Subsequently, 150 μl of supernatant was aspirated, and the absorbance at the wavelength of 545 nm was measured using a microplate reader. Three samples were measured and the average value was calculated. The hemolysis rate (HR) was calculated using the following formula:

$$HR = \frac{ODs - ODn}{ODp - ODn} * 100\%$$

ODs represents the absorbance value of the sample, ODn represents the mean absorbance value of the negative control group, and ODp represents the mean absorbance value of the positive control group. Samples with a hemolysis rate lower than 5% were considered eligible.

Cytocompatibility

In vitro culture of HUVECs

Passages 2-9 of HUVECs (PCS-100-010, ATCC, USA) were used and cultured in an incubator at 37°C and 5% CO_2. The medium used consisted of 500 ml of ECM, 25 ml of FBS, 5 ml of P/S, and 5 ml of ECGS (1001, Sciencell, USA). When the cells reached 75% to 80% confluence in the culture flask, they were collected for the subsequent experiment.

Preparation of endothelial cell culture medium (ECM) extract

Control, Mg substrate, Mg-OH, and Mg-$(SA/CMCS)_6$ groups were established. The alloy sheets were placed into the 24-well plates with 1 piece per well. ECM medium was added to each well at a standard volume of 1 ml/cm^2 and then incubated at 37°C and 5% CO_2 for 24 h to obtain extracts. The control group was only added with culture medium for 24 h.

Proliferation assay

In the 96-well plates, Control, Mg substrate, Mg-OH, and Mg-$(SA/CMCS)_6$ groups were set up with 100 μl of cell-containing medium added to each well at a cell density of 2×10^3 cells/well and each test was conducted in quadruplicate. After overnight culture, the medium in each group was replaced with the corresponding extract, and ECM containing 10% CCK-8 reagent was added. After being washed with PBS, the plates were incubated in an incubator for 3 h. The OD value at the wavelength of 450 nm was measured using a microplate reader.

NO release

HUVECs were seeded in 96-well plates at a density of 2×10^3 cells/well and each test was conducted in triplicate. After overnight culture, the medium in each group was changed to the corresponding extract. The medium supernatant was collected at 1 d, 3 d, and 5 d of culture following the instructions of the NO assay kit (S0021S, Beyotime, China). The absorbance at the wavelength of 540 nm was measured using a microplate reader to generate a standard curve and calculate the NO concentration in the supernatant sample.

Cell scratch assay

HUVECs were seeded at a density of 4×10^5 cells/well in 6-well plates and cultured using normal culture medium. Each test was conducted in triplicate. When the cell density reached about 95%, a 200 μl tip was used to create a scratch. Each well was washed gently six times with 1 ml of PBS, and then 2 ml of the corresponding group extract was added to each well. Cell migration was documented by photography using an inverted microscope (DMi8, Leica, Germany) at 0 h and 6 h of continuous culture and quantified using Image J software.

Transwell

Cell culture inserts (353097, BD Falcon, USA) for 24-well plates were used as the upper chamber, while 24-well plates served as the lower chamber. In the 24-well plates, 700 μl of the corresponding group extract was added. HUVECs were resuspended in serum-free ECM medium and added to the upper chamber at a seeding density of 6×10^4 cells/well and each test was conducted in triplicate. After 48 h of incubation, the upper chamber medium was discarded, and the inserts were washed three times with PBS. Migrated cells were fixed with 4% paraformaldehyde and stained Crystal Violet-Gentian et Stain Solution. The cells were observed and photographed under an inverted microscope, and the number of cells was calculated using Image J software.

Angiogenesis test

Matrigel was mixed with culture medium at a ratio of 2:1 and added to 96-well plates at 50 μl per well. The plates were then incubated at 37°C for 1 h. HUVECs were resuspended in the corresponding extract and added to the 96-well plates at a density of 3.5×10^4 cells per well with 50 μl. Each test was conducted in quadruplicate. After incubation at 37°C for 6 h, HUVEC angiogenesis was photographed, recorded, and analyzed using Image J software.

Immunofluorescence staining

Cell slides were placed in 24-well plates, HUVECs were seeded at a density of 4×10^4 cells per well and each test was conducted in triplicate. After overnight incubation, the old medium was replaced with the corresponding group extract. After 48 h, the cells were fixed with 4% para-formaldehyde, permeabilized with 0.25% Triton X-100, and added goat serum to block the samples. Subsequently, anti-VE-cadherin antibody (1:100) and anti-vWF antibody (1:250) were added separately, and the samples were incubated overnight at 4°C. The next day, Alexa Fluor® 488 fluorescent antibody and Alexa Fluor® 647 fluorescent antibody were added and incubated at 37°C for 1 h in the dark. Then the fluorescent mounting medium (containing DAPI) was used for nuclear staining and mounting for 30 min in the dark. Confocal laser scanning microscopy (STELLAR5, Leica, Germany) was used to observe and photograph the samples.

In vitro culture of HCASMCs

Passages 2-9 of HCASMCs were used and cultured in an incubator at 37°C and 5% CO_2. The medium used consisted of 500 ml of SMCM, 25 ml of FBS, 5 ml of P/S, and 5 ml of SMCGS (1101, Sciencell, USA).

Transwell

HUVECs were added to the 24-well plates at a density of 8×10^4 cells per well. After overnight incubation, the medium was changed to the corresponding extract for 48 h. Then, the cells were placed in the upper chamber. HCASMCs resuspended in serum-free SMCM medium were added to the upper chamber at a density of 6×10^4 cells per well. Each test was conducted in triplicate. The remaining steps were as previously described.

In vitro culture of THP-1

Control, Mg substrate, Mg-OH, and Mg-(SA/CMCS)$_6$ groups were set up. THP-1 cells were cultured in a cell incubator at 37°C with 5% CO_2. RPMI-1640 complete medium (338360, BNCC, China) was used to culture the cells. THP-1 cells were seeded into 6-well plates at a density of 4×10^5 cells per well and cultured overnight. Then, the medium was changed to 2 ml of each group extract containing 7 ng/ml PMA for 24 h to induce adherence to M0 macrophages. The old medium was removed, and 2 ml of each group extract containing 0.5 μl/ml IFN and 1 μl/ml LPS was added to induce M1 macrophages. Similarly, M2 macrophages were induced with 2 ml of each group extract containing 0.2 μl/ml IL-4. Each group was cultured for 48 h and each test was conducted in triplicate.

ELISA for IL-6/IL-10

The supernatant of M0/M1/M2 macrophages in each well was collected and centrifuged at 1000 g for 20 min. IL-6/IL-10 detection was performed using the IL-6/IL-10 enzyme-linked immunosorbent assay kit (m1028583-C/m1028605-C, mlbio, China).

Detection of inflammation-related genes by qRT-PCR

M0/M1/M2 macrophages were collected from each well. Total RNA was extracted using the FastPure® Cell/Tissue Total RNA Isolation Kit V2 (RC112, Vazyme, China), then reverse transcribed using the HiScript® III RT SuperMix for qPCR (R323-01, Vazyme, China). The expression of Arg-1, ODC-1, TNF-α, Arg-2, and Netrin-1 genes in M0, M1, and M2 macrophages were detected using Taq Pro Universal SYBR Master qPCR Mix (Q712, Vazyme, China) on an ABI StepOne real-time PCR machine (ThermoFisher Scientific, USA).

QUANTIFICATION AND STATISTICAL ANALYSIS

Data analysis was performed using GraphPad Prism 9 statistical software. The measurement data conforming to a normal distribution were described as (mean ± SD). The comparison between multiple groups was analyzed by Two-way ANOVA. Statistical significance was defined as P<0.05 and recorded as * , P<0.01 and recorded as ** , and P<0.001 and recorded as ***.